Enhanced Hole Mobility in Regioregular Polythiophene Infiltrated in Straight Nanopores**

By *Kevin M. Coakley*, *Bhavani S. Srinivasan*, *Jonathan M. Ziebarth*, *Chiatzun Goh*, *Yuxiang Liu*, and *Michael D. McGehee**

We demonstrate that the hole mobility in regioregular poly(3-hexylthiophene) can be enhanced by a factor of 20 by infiltrating it into straight nanopores of anodic alumina. Optical characterization shows that the polymer chains are partially aligned in the charge-transport direction.

1. Introduction

Regioregular poly(3-hexylthiophene) (RR P3HT) is one of the most promising conjugated polymers for polymer-based photovoltaic (PV) cells.[1,2] This polymer has a higher mobility than most other polymers because it forms a semicrystalline lamellar structure during spin-casting. Since the chains in the crystalline regions of the film are relatively straight and π-stacked against each other, charge transport can occur both along the chains and between the chains, which enables holes to find pathways around defects and chain terminations. While field-effect transistor (FET) hole-mobility values close to 0.1 $cm^2V^{-1}s^{-1}$ have been obtained in P3HT,[3–5] the mobility of this polymer in the diode configuration at room temperature has been measured to be only 3×10^{-4} $cm^2V^{-1}s^{-1}$.[6,7] It is important to understand why the diode mobility is lower and to find a way to increase it, since it is the relevant mobility for light-emitting diodes (LED) and PV cells, which have charge transport in the direction perpendicular to the substrate. Blom and coworkers have shown that for disordered polymers such as poly(2-methoxy-5-(3′,7′-dimethyloctyloxy)-*p*-phenylene vinylene) (OC_1C_{10}-PPV), the hole mobility measured in the FET configuration is higher than that obtained in the diode configuration because the charge-carrier concentration is typically much higher in the transistor geometry. When the carrier concentration in the film is high, the deep charge-trapping states in the film are filled, leading to an increase in mobility.[8] However, for polymers like regioregular P3HT that form well-ordered films,[9] the difference in hole mobility that occurs in the two types of devices cannot be accounted for entirely by a change in carrier concentration, which strongly suggests that the anisotropy in hole transport in these materials results from the tendency of the polymer chains to lie in the plane of the substrate. For this reason, one possible route for achieving improved hole mobilities with a well-ordered polymer in a diode configuration is to align the polymer chains perpendicular to the substrate by confining them in vertically oriented nanopores. Tolbert and coworkers have used polarized absorption and emission measurements to show that conjugated polymers can be highly aligned in mesoporous silica films with sub-5 nm diameter pores.[10,11] In their most recent experiments the pores were oriented in the plane of the film, but electrical measurements were not reported.[12] In order to make films with nanopores oriented perpendicular to the substrate, we chose to use anodic alumina.[13–15] In this article we demonstrate that the chain orientation in P3HT is changed by infiltrating it into anodic alumina films with pore diameters in the range of 20–120 nm. We present two-dimensional device simulations which show that the charge-carrier density for polymer in the pores of the alumina is increased compared to a neat film because the screening effect of the dielectric leads to an increased hole concentration at the polymer/alumina interface. Finally, we show that, at an optimum pore size, the hole mobility in P3HT infiltrated into nanopores is improved significantly, by as much as a factor of 20 compared to a neat film, to 6×10^{-3} $cm^2V^{-1}s^{-1}$.

2. Results and Discussion

Anodic alumina is an excellent material for studying the properties of polymers in confined vertical channels[16,17] because the pores in the alumina run vertically towards the substrate, and because the pore diameter of the alumina can be varied over the range of 15–300 nm by adjusting the anodization voltage and acid electrolyte.[13–15] By measuring the porosity and the thickness of the anodic alumina films from scanning electron microscopy (SEM) images, the exact thickness of

[*] Prof. M. D. McGehee, Dr. K. M. Coakley, B. S. Srinivasan, C. Goh
Department of Materials Science and Engineering, Stanford University
Stanford, CA 94305 (USA)
E-mail: mmcgehee@stanford.edu
Dr. J. M. Ziebarth
Department of Electrical Engineering, Stanford University
Stanford, CA 94305 (USA)
Y. Liu
Department of Chemistry, Stanford University
Stanford, CA 94305 (USA)

[**] Kevin M. Coakley and Bhavani S. Srinivasan contributed equally to this work. The authors acknowledge the Global Climate and Energy Project at Stanford, the Henry and Camille Dreyfus Foundation, Nanosolar, and the National Science Foundation for funding this research. The authors also thank Nanosolar for providing the procedure to make anodic alumina films and Guleid Hussen (Stanford MSE) and Vignesh G. Shankar (Stanford MSE) for supplying aluminum-coated SnO_2:F substrates.

 DOI: 10.1002/adfm.200500364 © 2005 WILEY-VCH Verlag GmbH & Co. KGaA, Weinheim

polymer (RR P3HT) needed to fill the pores can be calculated. The required amount of polymer is spin-cast and infiltrated into the pores of anodic alumina templates using a melt-infiltration technique described elsewhere.[18] Figure 1 shows the top view and cross-sectional SEM images of an anodic alumina template with 20 nm pore diameters, as-prepared (Figs. 1a,b) and after the infiltration of P3HT and deposition of a gold top electrode (Fig. 1c). From the image of the sample after polymer infiltration, it is apparent that the polymer that was deposited on top of the anodic alumina substrate infiltrates to the bottom of the pores, since there is only a thin polymer overlayer on top of the anodic alumina structure. This guarantees that the electronic and optical properties of the film are determined by the polymer in the pores and not by the polymer on top of the alumina. X-ray photoemission spectroscopy (XPS) depth-profile studies (Fig. 2) also show that the polymer infiltrated to the bottom of the pores at all pore sizes. The fact that the carbon signal does not drop to zero until the silicon signal from the glass substrate starts to increase shows that polymer infiltrates to the bottom of the pores. Interestingly, for reasons that we do not yet understand, the polymer density is at a minimum half-way down the depth of the porous structure for the 20 nm pore-diameter anodic alumina film (Fig. 2a). In contrast, for the other pore sizes the carbon signal only declines very slightly through the thickness of the anodic alumina film (Figs. 2b,c).

The strong tendency of conjugated polymer chains to lie in the plane of the substrate in a neat film was first observed by McBranch et al.,[19] who determined the anisotropy of the poly-

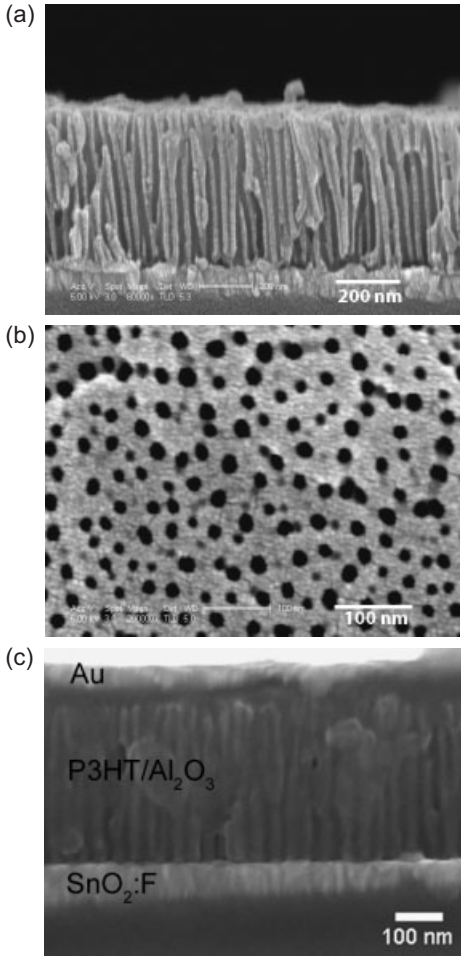

Figure 1. SEM images of anodic alumina. a) Cross-section view of as-fabricated 20 nm pores. b) Top view of as-fabricated 20 nm pores. c) Cross-section view after infiltration of P3HT and deposition of a gold top electrode. A thin layer of gold was sputtered on top of the anodic alumina before imaging to minimize charging effects for (a,b).

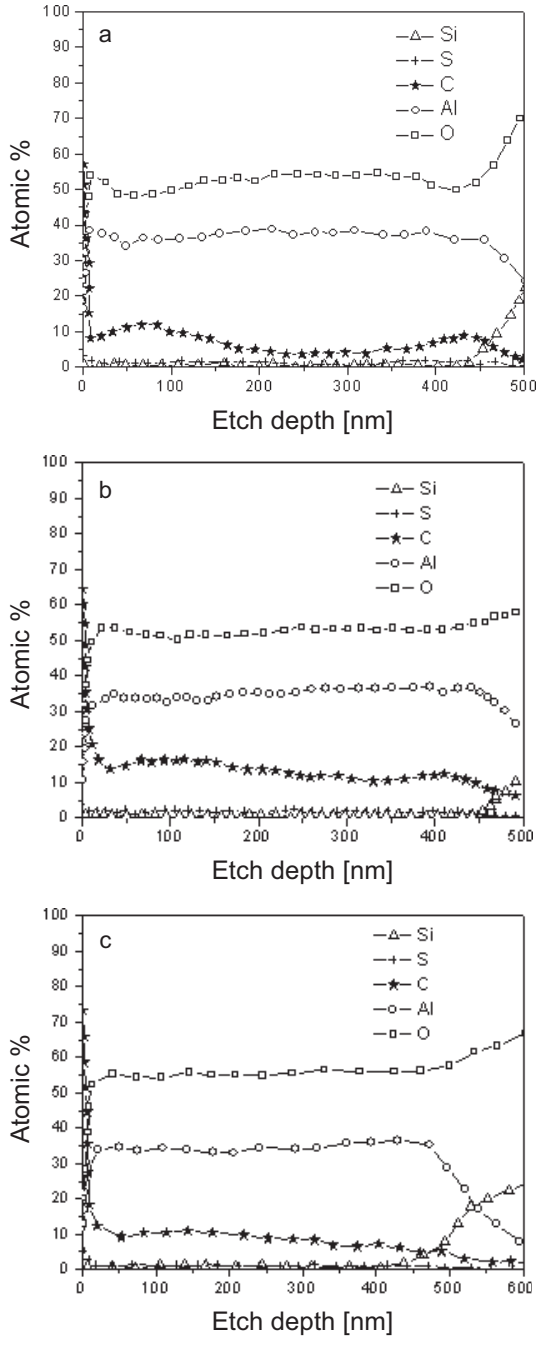

Figure 2. XPS depth profiles of P3HT in anodic alumina with a) 20 nm diameter pores, b) 40 nm diameter pores, and c) 75 nm diameter pores.

 © 2005 WILEY-VCH Verlag GmbH & Co. KGaA, Weinheim

ADVANCED FUNCTIONAL MATERIALS

mer chains by measuring the imaginary indices of refraction for light traveling with its electric field polarized in- and out-of-plane of the polymer film. This technique makes use of the fact that conjugated polymer chains are much more polarizable along their length and that consequently the absorption transition is stronger when the electric field is parallel to the chains. We used this optical method, depicted schematically in Figure 3a, to determine the orientation of the infiltrated polymer chains in the pores of the anodic alumina. Figure 3c shows the angle-dependent coefficients of transmission and reflection for p-polarized 514 nm light for a neat film of P3HT. By fitting this data to a three-layer transfer matrix model[20] that included the complex index of refraction of the absorbing layer, we extracted the absorption coefficients for light traveling with the electric field in the plane of the film, $\alpha_{\parallel}$, and for light traveling with the electric field out of the plane of the film, $\alpha_{\perp}$. We found that $\alpha_{\perp} = 0.19\alpha_{\parallel}$, which confirms that P3HT chains lie mostly in the plane of the film. Figure 3d shows the angle-dependent transmission and reflection data for P3HT infiltrated into anodic alumina with 75 nm pores. In this case, the transfer matrix model shows that $\alpha_{\perp} = 0.77\alpha_{\parallel}$. The substantial reduction in the absorption anisotropy shows that the polymer chains are more oriented in the vertical direction when inside the 75 nm pores. Figure 3b shows $\alpha_{\perp}/\alpha_{\parallel}$ as a function of pore size. We see that for all pore sizes, the chains are more oriented in the vertical directions. When the pores are smaller than 60 nm in diameter, the orientation improves rapidly with decreasing pore size. It is possible that the partial alignment in the large pores arises from chains orienting along the pore walls and that the good alignment at small pore sizes arises when the chains, which are relatively rod-like, are too long to lie horizontally in the pores. Experiments with molecules of different sizes will be carried out to further elucidate why the polymer chains align in nanopores.

The current density–voltage (J–V) curves for hole-only diodes made from P3HT infiltrated into anodic alumina and for neat films of the polymer are shown in Figure 4. In these devices, ohmic hole injection is achieved through a gold top electrode, and fluorine-doped tin oxide is used as a bottom electrode. As can be seen from Figure 4, the current density, which is calculated by simply dividing the total current by the electrode area, is approximately 50 times larger when P3HT is infiltrated into a 300 nm thick film of anodic alumina than when it is in a 300 nm thick neat film. The increase in current occurs despite the fact that the presence of the insulating alumina reduces the effective cross-sectional area of the conducting polymer regions beneath the top electrode of the anodic alumina

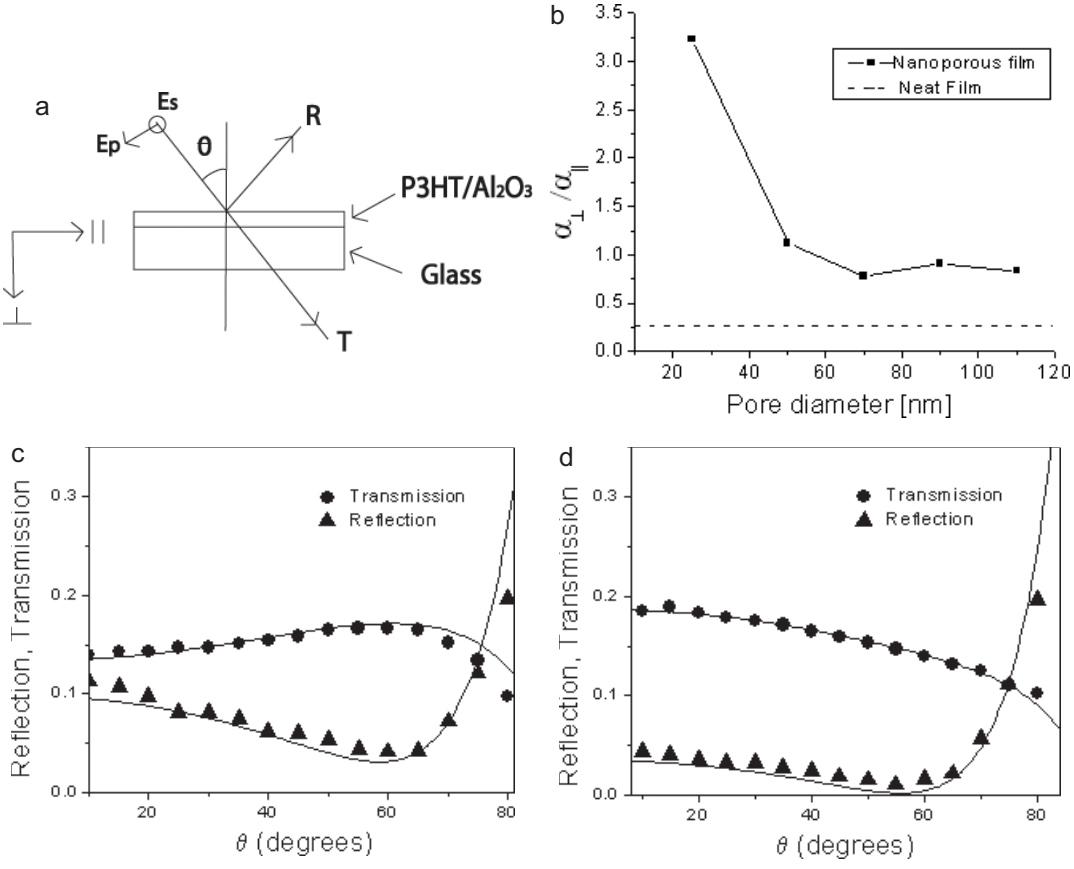

Figure 3. Optical determination of polymer chain alignment in anodic alumina nanopores. a) Schematic illustration of the experimental setup. b) Plot of $\alpha_{\perp}/\alpha_{\parallel}$ as a function of pore diameter. c) Coefficients of reflection and transmission for a neat film of P3HT under p-polarized 514 nm illumination. d) Coefficients of reflection and transmission for P3HT infiltrated into anodic alumina with 75 nm-diameter pores under p-polarized 514 nm illumination. Solid lines represent the best fit to the experimental data. E_s: electric field polarized in the plane of the film; E_p: electric field polarized out of the plane of the film; R: reflection coefficient; T: transmission coefficient.

 © 2005 WILEY-VCH Verlag GmbH & Co. KGaA, Weinheim

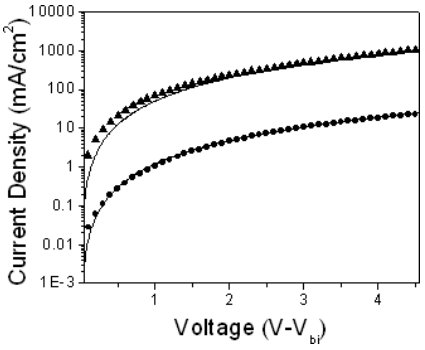

Figure 4. Current density–voltage curves for neat film and infiltrated polymer devices. *J–V* curves for P3HT in the 75 nm diameter pores of anodic alumina (triangles) and in a neat film of P3HT (circles). Solid lines illustrate the V^2 dependence of the *J–V* curves. The built-in volatage (V_{bi}) was measured to be between 0.9 and 1.2 V for the devices.

device. In both cases, J is proportional to V^2, which is in accordance with the space charge limited current (SCLC) model

$$J = \frac{9}{8}\varepsilon_o \varepsilon_r \mu \frac{V^2}{L^3} \quad (1)$$

(where ε_o is permitivity of free space, ε_r is the dielectric constant, μ is the mobility, V is potential, and L is the thickness) with no field-dependence in the mobility above the built-in voltage of the diode. However, before we conclude from these *J–V* curves that the hole mobility is higher when the polymer is infiltrated into a vertical channel template, we must first account for the possibility that the insulating alumina regions of the film might have a charge-screening effect on the holes injected into the polymer regions of the film. This could lead to an enhancement in the current without an increase in the hole mobility.

In order to quantify how the presence of the alumina dielectric affects charge transport in the infiltrated polymer, we modeled hole transport through the structure in cylindrical coordinates using the two-dimensional device simulator Medici, which determines the potential profile, carrier profile, and current flow through a user-defined device structure by solving the Poisson equation and continuity equation simultaneously. Figure 5a shows a two-dimensional contour plot of the electrical potential drop through a cylindrical polymer region with a 500 nm diameter surrounded by a ring-shaped alumina region and a concentric outer polymer region under an applied external potential of 10 V. (We note that even though we did not typically use pore diameters as large as 500 nm or voltages as high as 10 V in our real devices, we include the simulation result shown in Figure 5a in order to demonstrate the key effect that the alumina has on the potential profile in the polymer during device operation.) At the center of the alumina regions, the potential drops linearly with depth (Fig. 5b), as is to be expected in an insulator with no free carriers. On the other hand, in the center of the polymer region, the presence of holes in the film causes the potential to drop in proportion to depth$^{3/2}$, as should occur in this region of the device when it is operating in the SCLC regime. An important consequence of the poten-

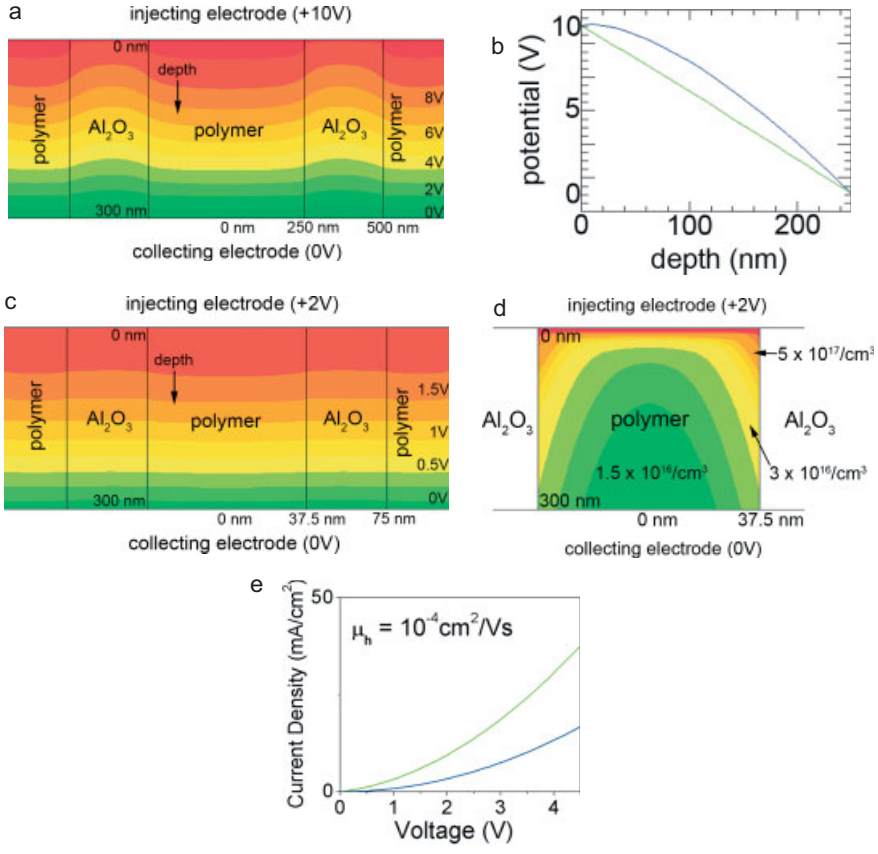

Figure 5. Two-dimensional device model for a conjugated polymer inside a column of porous alumina. a) Two-dimensional contour plot of potential versus radius and depth for an applied voltage of 10 V and a 500 nm pore diameter. b) One-dimensional plot of the potential drop versus depth at r = 0 nm (blue curve) and r = 375 nm (green curve) for the device structure shown in (a). c) Two-dimensional contour plot of potential versus radius and depth for an applied voltage of 2 V and a 75 nm pore diameter. d) Two-dimensional contour plot of the hole concentration in a 75 nm diameter pore under an applied voltage of 2 V. e) Simulated current density through a polymer that is surrounded by a dielectric ring (green curve) and for a neat film of the same area (blue curve). The hole mobility is 10^{-4} cm^2/Vs in both cases. Both the dielectric screening effect and the ~60% reduction in conducting area that arises from the presence of insulating alumina regions in the film are accounted for in this plot.

 © 2005 WILEY-VCH Verlag GmbH & Co. KGaA, Weinheim

ADVANCED FUNCTIONAL MATERIALS

tial not being the same in the polymer and dielectric regions at a given depth is that there is a lateral electric field in the film that drives holes to the polymer/dielectric interface. For the more realistic case of the potential drop through a film with 75 nm pore diameters and an applied voltage of 2 V (Fig. 5c), the presence of a lateral electric field in the film results in the build-up of charge at the polymer/dielectric interface, as shown in Figure 5d. This effect arises because the holes in the polymer region repel each other, but the repulsion from holes in neighboring channels of polymers is screened by the alumina dielectric. For a given applied voltage, the device simulation shows that the hole concentration is greater in the polymer region when it is surrounded by a dielectric than in a neat film. Consequently, the calculated current density is higher even if the hole mobility is the same. Figure 5e shows that if both this dielectric screening effect and the ~60 % reduction in conducting area that arises from the presence of insulating alumina regions in the film are accounted for, the current density through a 300 nm thick vertical channel device with 75 nm diameter pores will be 2.5 times larger than through a 300 nm thick neat film with the same hole mobility. The aspect ratio of the pores also causes a deviation from the usual L^3 dependence of SCLC.[21] These geometric and screening effects must be accounted for when extracting the hole mobility from J–V curves for these nanoporous diodes.

We find that the enhanced current observed in vertical channel devices is much too large to be accounted for solely by the dielectric screening effect of the alumina. In a sample with 75 nm diameter pores, we conclude that the hole mobility is enhanced over that of a neat film by a factor of 20, to 6×10^{-3} $cm^2V^{-1}s^{-1}$. We see no apparent field dependence in the mobility in our devices. In addition, the current through the vertical channel device is much larger than the current through the neat film even at very low applied voltages and correspondingly low carrier concentrations throughout the devices. Based on these two factors, we rule out the possibility that these devices are operating in a regime where carrier concentration significantly affects the mobility.[8,9] This strongly suggests that the increased mobility in the vertical channel device results primarily from the relative alignment of the chains of P3HT in the pores along the charge-transport direction as compared to a neat film. Despite the fact that the average vertical chain alignment is not very good, we hypothesize that the large enhancement in mobility occurs because most of the holes travel near the polymer/alumina interface, where the chains are probably well aligned and ordered.

Figure 6 shows the hole mobility of P3HT infiltrated into 300 nm thick alumina films as a function of the pore diameter in the alumina. For all the data points, we accounted for the dielectric screening effect, the aspect ratio of the pores, and the fractional area occupied by the polymer in order to extract the hole mobility from J–V curves accurately. For pore diameters in the range 50–75 nm, a strongly enhanced mobility is observed, with the highest measured mobility value equal to 6×10^{-3} $cm^2V^{-1}s^{-1}$. For pore diameters above 75 nm, the hole mobility falls off and approaches the mobility value measured for a neat film of P3HT (3×10^{-4} $cm^2V^{-1}s^{-1}$), as expected. Surprisingly, when the pore diameter is decreased below 60 nm, the hole mobility decreases substantially, which is counterintuitive because the optical data suggests that vertical alignment of the polymer chains increases as the pore size decreases. It is likely that the polymer chains do not pack as well on each other or that the pathways for current are disrupted in the smaller pores. Experiments are underway to better understand the dependence of mobility on pore size.

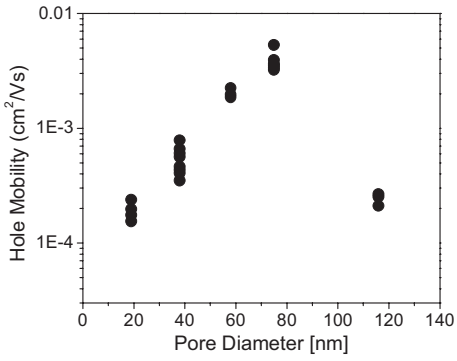

Figure 6. Hole mobility in P3HT infiltrated into anodic alumina as a function of the pore diameter in the alumina.

3. Conclusions

Our results have important implications for bulk heterojunction PV cells that consist of organic and inorganic semiconductors patterned around each other at the 10 nm length scale.[22–24] The fact that the hole mobility in P3HT can be enhanced by aligning the chains along the inorganic surface is important because the quantum efficiency of many bulk heterojunction PV cells is limited by hole transport through the conjugated polymer.[22,25–27] Although we observed a decrease in the P3HT hole mobility as the pore size approached the 10 nm length scale, we believe that this effect might be overcome by improving the polymer infiltration and the polymer chain morphology near the pore walls. Our device simulations show that holes are concentrated at the edge of the pore wall. If the insulating alumina was replaced by a semiconductor that carried electrons, we would expect that electrons in this semiconductor would also pile up at the interface, which should enhance the rate of back-electron transfer. This effect should be considered when modeling bulk heterojunction PV cells.

4. Experimental

RR P3HT was obtained from Aldrich and purified in a nitrogen atmosphere by Soxhlet extraction with hexane and chloroform, followed by the removal of chloroform under vacuum. The final product was dried at 45 °C under vacuum for 24 h. The number-average molecular weight (M_n) and polydispersity (PDI) of P3HT were 20 000 g mol^{-1} and 2.0, respectively.

To make the anodic alumina films with varying pore diameters, we deposited 300 nm thick films of aluminum on fluorine-doped tin oxide (SnO_2:F) substrates and anodically etched the aluminum at constant voltage. The voltage we used for a given sample was varied from 15 to 75 V depending on the desired pore spacing. After anodizing the alu-

 © 2005 WILEY-VCH Verlag GmbH & Co. KGaA, Weinheim

minum, we performed a wet etch using 1 M phosphoric acid on all samples to widen the pores and expose the SnO_2:F bottom electrode by removing the barrier alumina layer at the bottom of the pores. The etched films were then rinsed thoroughly in water, dried, and characterized with SEM image analysis software to obtain the average pore size and porosity for each anodization voltage. In order to infiltrate conjugated polymers into the pores of the alumina, a layer of P3HT was spin-cast on top of the alumina from tetrahydrofuran (THF), heated at 200 °C for 1 min, and then cooled slowly to room temperature. In order to maintain a consistent thermal history for all devices, neat film devices were given the same thermal treatment. Following evaporation of a gold top electrode, devices were typically annealed at 100 °C for several hours to achieve optimized hole injection through the top electrode.

Optical measurements were made using either neat films of polymer on glass substrates, or films of polymer infiltrated into anodic alumina on glass substrates. In the case of the anodic alumina samples, we gently wiped the samples with a toluene-soaked cotton swab before optical characterization in order to ensure that there was no polymer overlayer on top of the alumina. To determine the indices of refraction of neat and infiltrated films, we first measured the transmission and reflection coefficients of the film as a function of incident angle and polarization using a two-ring rotation stage. We used a 531 nm green diode laser or a 514 nm Ar ion laser as excitation sources. The measured coefficients were then fitted to a 3-layer transfer matrix model for the dielectric stack using a least-squares fitting routine, which yielded the best-fit values for the complex indices of refraction of the absorbing layer for both s- and p-polarized light.

All device simulations were performed in cylindrical coordinates using Medici, a commercially available two-dimensional device simulator. We assumed a dielectric constant of 3 for the polymer region and 11 for the alumina region, which represents one of the highest reported values for alumina and hence yields a lower limit for the extracted hole mobility. In order to best account for the effect of the presence of holes in neighboring alumina channels besides the channel of interest, which act to reduce the screening effect that the alumina has on the main channel, we simulated a two-ring structure consisting of an outer ring of polymer, an inner ring of alumina, and an inner column of polymer. This resulted in a reduction in the dielectric screening factor by a factor of 2.3 compared to an isolated cylinder of polymer. In order to compensate for the fact that the polymer filling a central pore is not surrounded by a continuous outer ring of polymer in real devices, we used an alumina ring thickness that is twice the thickness of the real pore walls.

Depth profiling experiments were performed with a SSI S-Probe monochromatized XPS Spectrometer on anodic alumina films grown on glass substrates. X-rays were generated using Al Kα radiation (1486 eV). Sample etching was performed in situ using a Leybold Hereaus argon ion etcher with a 10 mA emission current. The incident angle of the rastered ion beam was 35°. The etch crater was 2 mm by 2 mm in size. In order to prevent edge sampling an X-ray spot size of 250 μm × 750 μm was used.

Received: June 12, 2005
Final version: August 22, 2005
Published online: October 31, 2005

[1] H. Hoppe, S. N. Sariciftci, *J. Mater. Res.* **2004**, *19*, 1924.
[2] K. M. Coakley, M. McGehee, *Chem. Mater.* **2004**, *16*, 4533.
[3] Z. Bao, A. Dodabalapur, A. J. Lovinger, *Appl. Phys. Lett.* **1996**, *69*, 4108.
[4] H. Sirringhaus, N. Tessler, R. H. Friend, *Science* **1998**, *280*, 1741.
[5] J. F. Chang, B. Q. Sun, D. W. Breiby, M. M. Nielsen, T. I. Solling, M. Giles, I. McCulloch, H. Sirringhaus, *Chem. Mater*. **2004**, *16*, 4772.
[6] C. Goh, R. J. Kline, M. D. McGehee, E. N. Kadnikova, J. M. J. Frechet, *Appl. Phys. Lett.* **2005**, *86*, 122 110.
[7] A. J. Mozer, S. N. Sariciftci, *Chem. Phys. Lett.* **2004**, *389*, 438.
[8] C. Tanase, E. J. Meijer, P. W. M. Blom, D. M. de Leeuw, *Phys. Rev. Lett.* **2003,** *91*, 216 601.
[9] C. Tanase, P. W. M. Blom, D. M. de Leeuw, E. J. Meijer, *Phys. Status Solidi A* **2004**, *201*, 1236.
[10] J. Wu, A. F. Gross, S. H. Tolbert, *J. Phys. Chem. B* **1999**, *103*, 2374.
[11] T.-Q. Nguyen, J. Wu, V. Doan, B. J. Schwartz, S. H. Tolbert, *Science* **2000**, *288*, 652.
[12] W. C. Molenkamp, M. Watanabe, H. Miyata, S. H. Tolbert, *J. Am. Chem. Soc.* **2004**, *126*, 4476.
[13] A. P. Li, F. Muller, A. Birner, K. Nielsch, U. Gosele, *J. Appl. Phys.* **1998**, *84*, 6023.
[14] M. S. Sander, L. S. Tan, *Adv. Funct. Mater.* **2003**, *13*, 393.
[15] K. Nielsch, J. Choi, K. Schwirn, R. B. Wehrspohn, U. Gosele, *Nano Lett.* **2002**, *2*, 677.
[16] C. R. Martin, *Science* **1994**, *266*, 1961.
[17] Z. H. Cai, J. T. Lei, W. B. Liang, V. Menon, C. R. Martin, *Chem. Mater.* **1991**, *3*, 960.
[18] K. M. Coakley, Y. Liu, M. D. McGehee, K. M. Frindell, G. D. Stucky, *Adv. Funct. Mater.* **2003**, *13*, 301.
[19] D. McBranch, I. H. Campbell, D. L. Smith, J. P. Ferraris, *Appl. Phys. Lett.* **1995**, *66*, 1175.
[20] J. Chilwell, I. Hodgkinson, *J. Opt. Soc. Am. A.* **1984**, *1*, 742.
[21] M. A. Lampert, P. Malik, *Current Injection in Solids*, Academic, New York **1970**.
[22] K. M. Coakley, M. D. McGehee, *Appl. Phys. Lett.* **2003**, *83*, 3380.
[23] W. U. Huynh, J. J. Dittmer, A. P. Alivisatos, *Science* **2002**, *295*, 2425.
[24] B. Q. Sun, E. Marx, N. C. Greenham, *Nano Lett.* **2003**, *3*, 961.
[25] J. K. J. van Duren, V. D. Mihailetchi, P. W. M. Blom, T. van Woudenbergh, J. C. Hummelen, M. T. Rispens, R. A. J. Janssen, M. M. Wienk, *J. Appl. Phys.* **2003**, *94*, 4477.
[26] W. U. Huynh, J. J. Dittmer, N. Teclemariam, D. J. Milliron, A. P. Alivisatos, K. W. Barnham, *Phys. Rev. B* **2003**, *67*, 115 326.
[27] S. A. Choulis, J. Nelson, Y. Kim, D. Poplavskyy, T. Kreouzis, J. R. Durrant, D. D. C. Bradley, *Appl. Phys. Lett.* **2003**, *83*, 3812.

 © 2005 WILEY-VCH Verlag GmbH & Co. KGaA, Weinheim